J. Fluid Mech. (2020), *vol.* 884, A16. © Cambridge University Press 2019
doi:10.1017/jfm.2019.932

Control of radial miscible viscous fingering

Vandita Sharma[1], Sada Nand[1], Satyajit Pramanik[2], Ching-Yao Chen[3,†] and Manoranjan Mishra[1,†]

[1]Department of Mathematics, Indian Institute of Technology Ropar, 140001 Rupnagar, India

[2]NORDITA, Royal Institute of Technology and Stockholm University, SE 106 91 Stockholm, Sweden

[3]Department of Mechanical Engineering, National Chiao Tung University, Hsinchu, Taiwan, 30010 Republic of China

(Received 28 June 2019; revised 20 September 2019; accepted 2 November 2019)

We investigate the stability of radial viscous fingering (VF) in miscible fluids. We show that the instability is determined by an interplay between advection and diffusion during the initial stages of flow. Using linear stability analysis and nonlinear simulations, we demonstrate that this competition is a function of the radius r_0 of the circular region initially occupied by the less-viscous fluid in the porous medium. For each r_0, we further determine the stability in terms of Péclet number (Pe) and log-mobility ratio (M). The Pe–M parameter space is divided into stable and unstable zones: the boundary between the two zones is well approximated by $M_c = \alpha(r_0) Pe_c^{-0.55}$. In the unstable zone, the instability is reduced with an increase in r_0. Thus, a natural control measure for miscible radial VF in terms of r_0 is established. Finally, the results are validated by performing experiments that provide good qualitative agreement with our numerical study. Implications for observations in oil recovery and other fingering instabilities are discussed.

Key words: convection in porous media, Hele-Shaw flows, fingering instability

1. Introduction

Hydrodynamic instabilities are ubiquitous to transport in porous media. Viscous fingering (VF) is one of these instabilities, which is observable while displacing a less-mobile fluid by another more-mobile fluid through porous media, and it plays critical roles in enhanced oil recovery through miscible flooding/solvent drive (Lake 1989), chromatography separation (Guiochon *et al.* 2008), pattern formation (Li *et al.* 2009), medicines (Bhaskar *et al.* 1992), CO_2 sequestration (Moortgat 2016; Amooie, Soltanian & Moortgat 2017; Li *et al.* 2019), diffusion-limited aggregation (Witten & Sander 1981), mixing (Jha, Cueto-Felgueroso & Juanes 2011) and bacterial colonies (Callan-Jones, Joanny & Prost 2008).

While advection is necessary for VF, diffusion stabilises this instability in miscible systems. For a given pressure gradient, the advection velocity is uniform in a rectilinear flow, whereas in a radial flow the velocity is inversely proportional to the radial distance from the point of fluid injection. The effects of diffusion on

† Email addresses for correspondence: chingyao@mail.nctu.edu.tw, manoranjan@iitrpr.ac.in

stabilisation of miscible fingering instabilities both in the linear and nonlinear regimes have been well understood mainly in the context of rectilinear displacement flows (Homsy 1987; Pramanik & Mishra 2015). In radial VF, the effects of diffusion at the initial stages of the displacement have been studied by Tan & Homsy (1987), who concluded that the dispersion is strong enough to completely suppress the instability when the Péclet number $\sim O(1)$; otherwise, the displacement is always unstable. On the other hand, Chui, de Anna & Juanes (2015) observed shut down of the overall flow instability emerging from the dominance of diffusion over advection at the later stages of the flow. More recently, the diffusion-driven transition between the two regimes of VF has been captured (Videbæk & Nagel 2019). Thus, there are many facets of the competition between advection and diffusion in radial flows. In contrast to this, Bischofberger, Ramachandran & Nagel (2014) claimed that the viscosity ratio sets the velocity of the interface and three regimes of instability are obtained, for which the effects of diffusion are irrelevant. In this article, we show that the diffusion can never be neglected when dealing with miscible fluids. Initial stable displacement is the characteristic of dominant diffusion, which is equilibrated by advection at a later stage that is identified as the transition to an unstable state dominated by advection.

Further, we ask: can we control the competition between advection and diffusion to suppress the miscible radial VF? Diffusion, being an inherent property that depends on the displacing and displaced fluids, is difficult to tune; however, the advection can be suitably modified. Many studies focused on controlling VF (Dias *et al.* 2012; Zheng, Kim & Stone 2015; Yuan *et al.* 2019) utilised time-dependent strategies to control advection. However, we achieve the same by merely modifying the initial configuration of radial displacement flow. We consider different initial finite volumes of the displacing fluid in the porous medium, which is represented by an initial radial distance (r_0) of the interface from the centre of the porous medium. The effects of competition between advection and diffusion on the controllability of VF are parametrised in terms of r_0 and are explained through linear stability analysis (LSA) and compared with the corresponding nonlinear simulations (NLSs), supported by the result of a diligently designed experiment.

2. Mathematical model

The fluids considered are Newtonian, miscible, non-reactive with μ_l, μ_m as viscosity of the less- and the more-viscous fluid, respectively. The non-dimensional governing equations for the flow in a two-dimensional (2-D) homogeneous porous medium are constituted by the Darcy's law and the transport equation for the solute concentration c,

$$\boldsymbol{\nabla}\cdot\boldsymbol{u}=0, \tag{2.1}$$

$$\boldsymbol{u}=-\frac{1}{\mu(c)}\boldsymbol{\nabla}p, \quad \mu(c)=\mathrm{e}^{(1-c)M}, \tag{2.2}$$

$$\partial_t c+\boldsymbol{u}\cdot\boldsymbol{\nabla}c=\frac{1}{Pe}\nabla^2 c, \tag{2.3}$$

where p is the hydrodynamic pressure and $\boldsymbol{u}=(u,\,v)$ is the Darcy velocity vector. We use t_f, the total time of fluid injection, as the characteristic time, and $\sqrt{Qt_f}$ as characteristic length, where Q is the gap-averaged flow rate. Consequently, we obtain two non-dimensional parameters: the Péclet number, $Pe=Q/D$, and the log-mobility

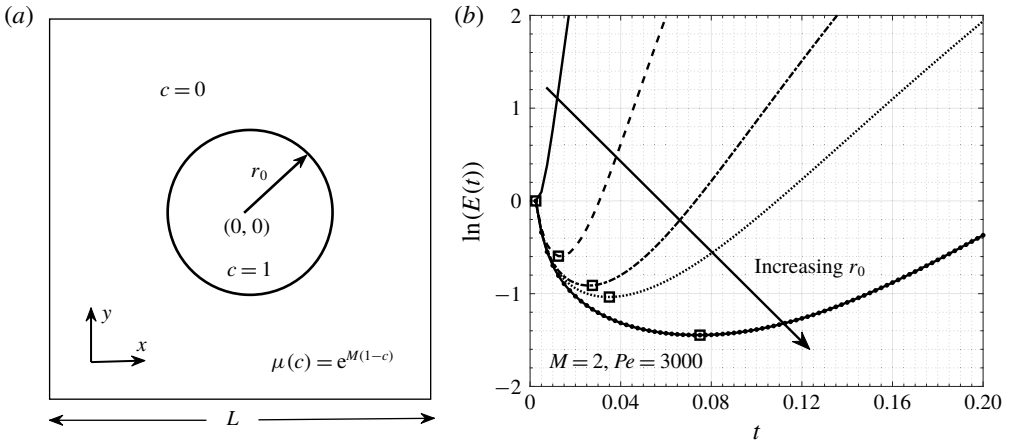

FIGURE 1. (*a*) Schematic of the computational domain $\Omega = [-L/2, L/2] \times [-L/2, L/2]$, with $L = 3$ used for LSA and NLS. The centre of the domain is chosen as the origin of the cartesian coordinate system and the source of the less-viscous fluid initially occupying a circle of radius r_0. Here $M > 0$. (*b*) Temporal evolution of $\ln(E(t))$ for $r_0 = 0.1$ to 0.3 with an increment 0.05. The onset time of instability is marked by □. The initial diffusion is prevalent for a longer time for a larger r_0 and, hence, the onset is delayed.

ratio, $M = \ln(\mu_m/\mu_l)$, where the molecular diffusion coefficient D of c in the solvent fluid is assumed to be a constant.

We consider a 2-D square domain Ω in the cartesian coordinates with the origin as the source of the less-viscous fluid (see figure 1*a* for computational domain). The initial condition associated with above equations is $\boldsymbol{u}(\boldsymbol{x}, t = 0) = \boldsymbol{x}/(2\pi|\boldsymbol{x}|^2)$ and

$$c(\boldsymbol{x}, t = 0) = \begin{cases} 1, & 0 \leqslant |\boldsymbol{x}|^2 \leqslant r_0^2 \\ 0, & \text{otherwise}, \end{cases} \tag{2.4}$$

where $\boldsymbol{x} = (x, y)$, and r_0 is the non-dimensional radius of the initial circle occupied by less-viscous fluid.

3. Linear stability analysis

We perform LSA to identify the effects of diffusion at the initial stages of the displacement and the onset of VF. Assume the base state velocity is $\boldsymbol{u}_b(\boldsymbol{x}) = \boldsymbol{x}/(2\pi|\boldsymbol{x}|^2)$, and the base state concentration c_b is the solution of (2.3) for the initial condition (2.4). An analytical solution for this initial boundary value problem is not attainable. Following the analysis of Tan & Homsy (1987) and Riaz, Pankiewitz & Meiburg (2004), we search the base state concentration in terms of similarity variables, which is a powerful, well-established technique to solve partial differential equations (PDEs). However, similarity solutions to PDEs are almost always independent of any specific initial condition (Ball & Huppert 2019). Owing to this and the fact that the novelty of our work in this article is to find stability in miscible VF in terms of the initial condition of the displacement flow, a base state solution in terms of similarity variables is inappropriate. We use the method of lines to numerically compute c_b. Spatial derivatives are discretised using sixth-order compact finite differences

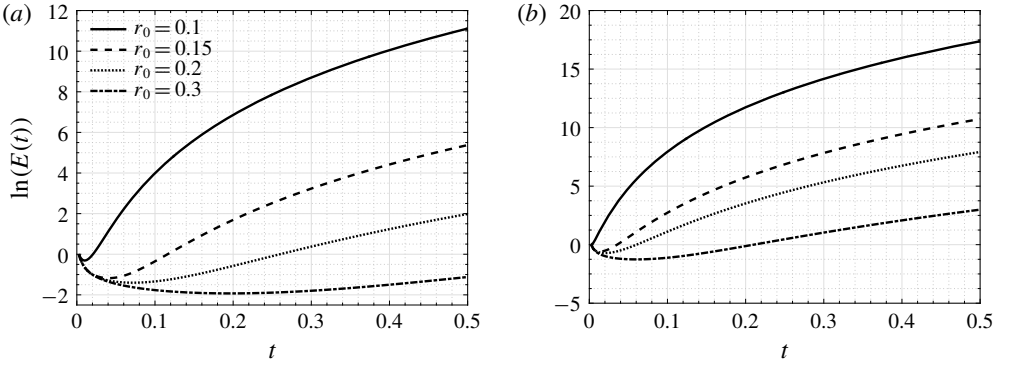

FIGURE 2. Natural logarithm of energy amplification as a function of time for (*a*) $M = 1$, $Pe = 5000$, and (*b*) $M = 3$, $Pe = 1000$.

(Lele 1992) and the resulting initial value problem is solved using a third-order Runge–Kutta method. The velocity field is solved in the form of a stream function $\psi(x, y)$, defined as $u = \partial_y \psi$, $v = -\partial_x \psi$.

We introduce an infinitesimal perturbation (ψ', c') such that $\psi = \psi_b + \psi'$, $c = c_b + c'$ $(|\psi'|, |c'| \ll 1)$, where ψ_b is the stream-function corresponding to $\boldsymbol{u}_b$. The corresponding linearised equations are solved for ψ', c' using the hybrid compact finite differences and the pseudo-spectral method. No flux boundary condition for c' and $\psi' = 0$ are used at the outflow boundary. The present LSA works as an alternative approach to study time-dependent linear system arising in miscible VF. Our interest does not lie in the wavelength selection like many other LSAs (Hota, Pramanik & Mishra 2015*a*), but in capturing initial diffusion and its effect on the onset of instability. However, it must be noted that our LSA is also applicable for wavelength selection (Hota, Pramanik & Mishra 2015*b*).

Recall that both c_b and c' evolve temporally. Therefore, the growth of c', ψ' are relative to those of c_b, ψ_b, and we quantify them at each instant of time. We define the energy ratio

$$R(t) = E_K(c', \boldsymbol{u}')/E_K(c_b, \boldsymbol{u}_b), \tag{3.1}$$

where $E_K(c, \boldsymbol{u}) = \int_\Omega [c^2 + \boldsymbol{u}^2] \, \mathrm{d}\Omega$ represents the kinetic energy at time t. The energy amplification,

$$E(t) = R(t)/R(t = 0), \tag{3.2}$$

is the ratio of the energy at time t to its value at $t = 0$ (Matar & Troian 1999). The nature of amplification as a function of time decides stability. An increasing or decreasing $E(t)$ indicates a relative growth or decay of the perturbations, while the presence of an extremum, if any, is of particular importance. A minimum indicates transition from a diffusion-dominating regime to an advection-dominated regime, which eventually implies the triggering of instability, whereas a maximum exhibits transient growths (Hota *et al.* 2015*a*). Figure 1(*b*) shows the natural logarithm of energy amplification as a function of time. Evidently, $\ln(E(t))$ is a non-monotonic function with a minimum occurring for each $r_0 > 0.1$. The minimum captures the competition between advection and diffusion in the linear regime. Up to the point of minimum, the disturbances are stabilised by the diffusive base state. The larger r_0, the later the point of minimum is obtained, indicating a delayed onset owing to the dominance of diffusive forces for a longer time. Similar qualitative results have been verified for various M and Pe as shown in figure 2. Therefore, our LSA captures controllability of VF owing to the competition between the two forces.

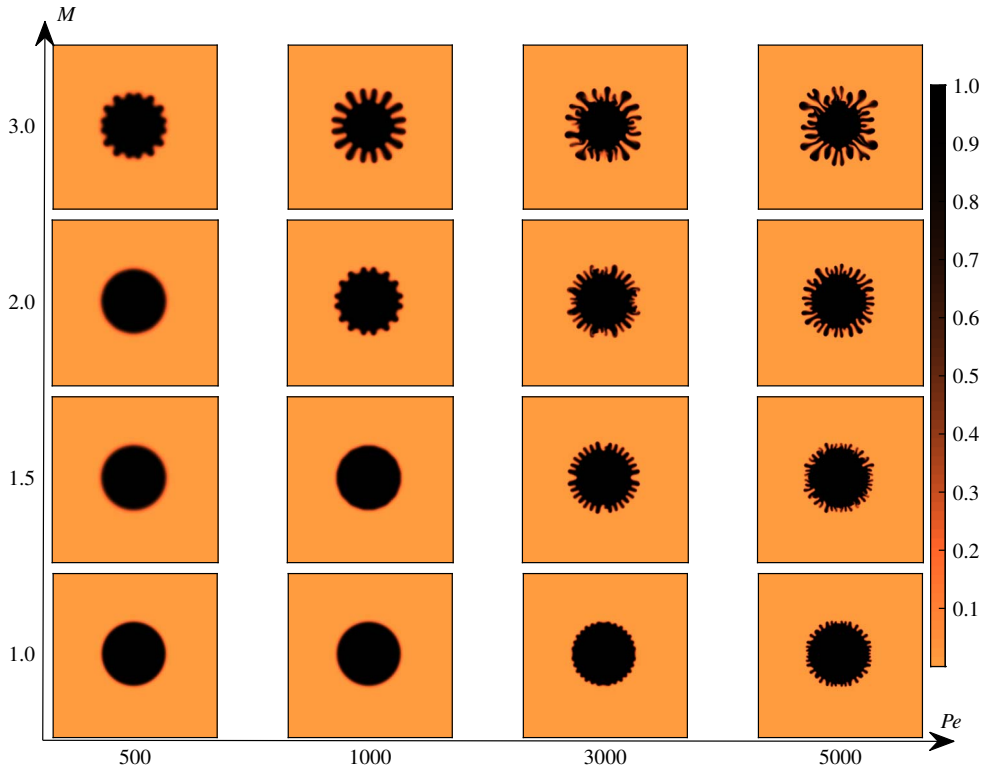

FIGURE 3. Density plots of concentration at $t = 1$ for $r_0 = 0.1$ and various M, Pe.

4. Nonlinear simulations

To support the estimates of LSA that the instability is delayed as r_0 increases, we perform NLS. We solve the coupled nonlinear equations (2.1)–(2.4) using a hybrid scheme based on compact finite differences and pseudo-spectral methods. This method has been used extensively to study instabilities in porous media (Chen *et al.* (2010), Sharma *et al.* (2019), and references therein). We perform NLS for five different values of r_0, and for each r_0, we consider $M \in [0, 3]$ and $Pe \in [500, 10^4]$. A range of fingering dynamics from intense fingering to no instability at all are visible in the density plots of the concentration in figure 3 for $r_0 = 0.1$ on varying M, Pe. Similar results are also observed for other r_0. Further, we explore the effect of r_0 on the fingering dynamics. A comparison of the concentration contours at a given time for the two radii in figure 4(*a*) clearly depicts that fingering instability is abated as r_0 increases. Thus, the NLSs support the instability control predicted by LSA and indicate the existence of stable displacements despite an unfavourable viscosity contrast (i.e. when a less-viscous fluid displaces a more-viscous fluid) and high Pe.

For each simulation, we compute the interfacial length (Mishra, Martin & De Wit 2008),

$$I(t) = \int_{\Omega} |\nabla c| \, \mathrm{d}\Omega, \tag{4.1}$$

which measures the temporal variation of the concentration gradient. In figure 4(*b*), we plot $I(t)$ normalised with its value at $t = 0$, for $Pe = 5000$. For $M = 0$, we analytically

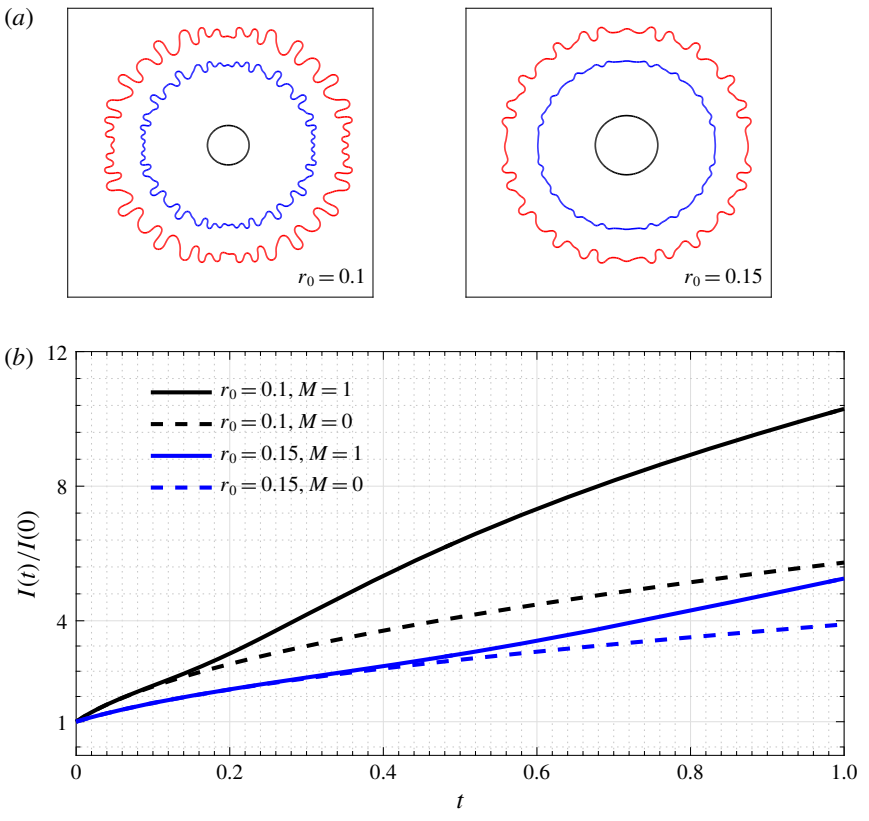

FIGURE 4. (*a*) Temporal evolution of concentration contour $c = 0.5$ for $Pe = 5000$, $M = 1$ with $t = 0$ (black), 0.5 (blue) and 1 (red). Increasing r_0 abates the instability as evident from the less-distorted contours at the same time for larger r_0. (*b*) Temporal evolution of normalised $I(t)$. Maiden deviation of the solid line ($M = 1$) from the dashed line ($M = 0$) marks the onset of instability.

calculate $I(t) = 2\sqrt{\pi(t + \pi r_0^2)} := I_0(t)$ (say); in the absence of VF, $I(t)$ must coincide with $I_0(t)$. Further, we define $\delta(t) = |I(t) - I_0(t)|/I_0(t)$ and plot $\delta(t = 1)$ versus M for $r_0 = 0.1$, $Pe = 3000$, 5000 in the inset of figure 5(*a*). It is observed that $\delta(t = 1) = 0$ for $0 \leqslant M \leqslant 0.75$ and $0 \leqslant M \leqslant 0.575$, respectively, for $Pe = 3000$ and 5000. This indicates $I(t)$ coincides with $I_0(t)$ even up to the final time for these parameters. Thus, for $M \in [0, 0.75]$, the displacement is stable despite an unfavourable viscosity contrast for $Pe = 3000$, $r_0 = 0.1$. Consequently, we use the value at the final time, $\delta(t = 1)$, to classify the parameter set as stable or unstable. If $\delta(t = 1) > 0$, the corresponding parameter set (r_0, M, Pe) is identified as unstable; otherwise, it is identified as stable. Here $M = 0.75$ and 0.575 lie on the boundary of the stable/unstable zone for $Pe = 3000$ and 5000, respectively, when $r_0 = 0.1$. Accordingly, for each r_0, we summarise the instability in the Pe–M parameter space in figure 5(*a*). This indicates that for a fixed M, there is a critical Péclet number (or, similarly for a fixed Pe, there is a critical log-mobility ratio) for the occurrence of instability. The existence of a critical parameter for fingering instability in radial source flow with a point source (i.e., $r_0 = 0$) has already been identified using LSA (Tan & Homsy 1987) and experiments (Bischofberger *et al.* 2014; Videbæk & Nagel 2019). Videbæk & Nagel (2019) provide critical parameters that determine transition in the fingering patterns

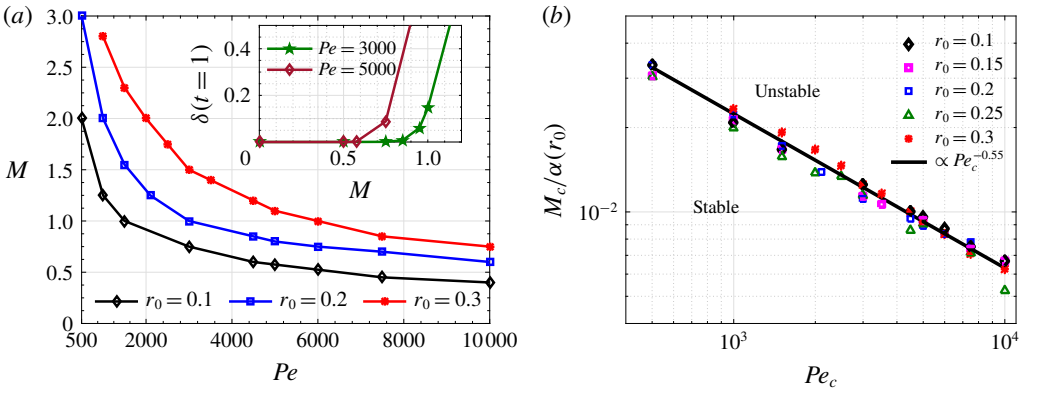

FIGURE 5. (*a*) The *M*–*Pe* parameter space divided into stable and unstable regions for each r_0. The ordered pair (Pe, M) below a curve corresponding to a given r_0 is associated with a stable displacement for the corresponding r_0. Inset: Plot of $\delta(t = 1)$ versus M for $r_0 = 0.1$. (*b*) Boundary between stable and unstable zones in the normalised M_c–Pe_c parameter space.

on account of diffusion. On the other hand, we are concerned with the transition between stability and instability, which arises due to competition between advection and diffusion. We would also like to emphasise that the initial condition in our study is different from that of Videbæk & Nagel (2019).

Another quantification of the competition between advection and diffusion is sought in terms of $I(t)$. An $I(t)$ identical to $I_0(t)$ indicates diffusion is the dominating force. We define $t = t_{on}$ as onset time of fingering in the nonlinear regime if $I(t) > I_0(t)$, for all t satisfying $t_{on} \lesssim t < 1$. Up to $t = t_{on}$, diffusion dominates advection and stabilises the displacement. For a larger r_0, the advection becomes weaker, consequently, t_{on} is more for $r_0 = 0.15$, the larger radius shown in figure 4(*b*). Furthermore, from NLS we observe that t_{on} increases with r_0 and the stable region spans over a larger range of both M and Pe. It is noteworthy that the boundary between the stable and unstable regions follow a scaling relation $M_c = \alpha(r_0) Pe_c^{-\beta}$, with $0.52 \lesssim \beta \lesssim 0.59$. We observe that for $\alpha(r_0) = 30(1 + 10r_0)$, the parameter pair (M_c, Pe_c) lying on the boundary between the stable and the unstable regions can be well approximated by the relation $M_c = \alpha(r_0) Pe_c^{-0.55}$ (figure 5*b*). Therefore, using this scaling relation we can approximate the stability of radial flows in homogeneous porous media.

5. Experiments

Our numerical results are further validated through state-of-the-art experiments. We used a radial Hele-Shaw cell with a gap width $b = 0.5$ mm. A hypodermic syringe needle (1.2 mm diameter and 40 mm length) bent in an L-shape and carefully embedded into a pipe was used to fill the two fluids in the Hele-Shaw cell. One may envision it as an annulus of L-shape pipe in straight outer pipe. The outer pipe is filled with more-viscous fluid while the inner pipe is filled with less-viscous fluid. This avoids the hassle of (a) changing the pipes for different fluids and (b) having a hole in each glass plate. A syringe pump (Cole-Parmer-D201253) was used for injecting the less-viscous fluid. Images were captured with a Sony FDR-AX40 camera. A schematic of the experimental set up is shown in figure 6. Aqueous glycerol

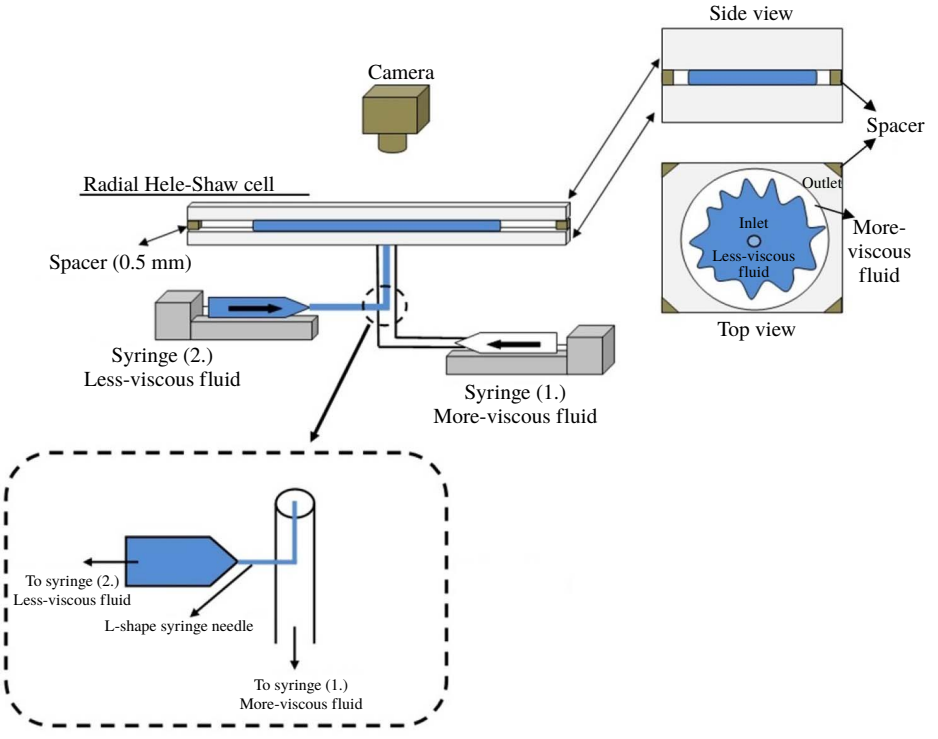

FIGURE 6. Schematic of the experimental set up, showing the concentric pipes to inject the two fluids.

Glycerol (Vol. %)	Water (Vol. %)	Viscosity of solution (mPa s)	M
58.33	41.67	11.26	0.504
71.43	28.57	31.14	1.521
77.78	22.22	53.05	2.053

TABLE 1. Aqueous glycerol solution with different percentage by volume for making more-viscous fluid.

(50 Vol. %) solution with viscosity 6.8 mPa s was used as the less-viscous displacing fluid. The displaced more-viscous fluid was prepared with different percentage by volume of glycerol solution as listed in table 1. The viscosity of different aqueous glycerol solution was measured by a rheometer (Anton-Paar: MCR-702) and found to be in agreement with the calculated value through the mathematical formulation given by Cheng (2008) and Volk & Kähler (2018).

To obtain the initial circle of radius $\bar{r}_0$, the less-viscous fluid was injected at a constant flow rate Q_1 µl s^{-1} for t_1 s in the Hele-Shaw cell, which was initially filled with the more-viscous fluid. The initial volume of the injected less-viscous fluid, $Q_1 t_1$ ml, was chosen so that it leads to a stable displacement of the more-viscous fluid until the invading fluid occupies a circular region of radius $\bar{r}_0$ mm. Recall that during this stable displacement, the interface between the two fluids experiences diffusive spreading proportional to a length $\sqrt{Dt_1}$, which also contributes in $\bar{r}_0$; we

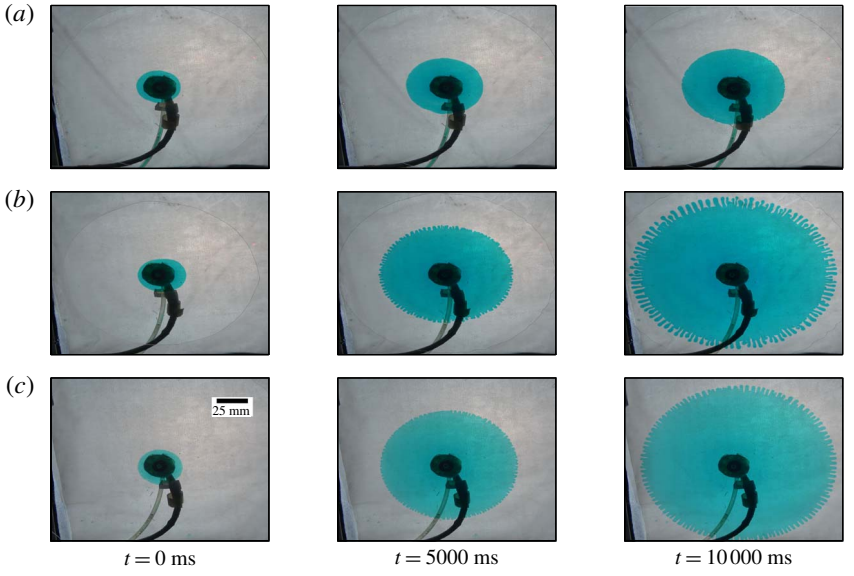

FIGURE 7. Images from the experiments at different times for $\bar{r}_0 = 18$ mm: (*a*) $M = 2.053$, $Q^* = 0.1$ ml s^{-1}, (*b*) $M = 2.053$, $Q^* = 0.5$ ml s^{-1} and (*c*) $M = 1.521$, $Q^* = 0.5$ ml s^{-1}. Pipes used for injecting the two fluids are also visible in the images. The black circle at the centre is the adhesive used for fixing the pipes to the Hele-Shaw cell.

measure $\bar{r}_0 = \sqrt{Dt_1} + \sqrt{Q_1 t_1/(\pi b)}$. Here, $D = 10^{-9}$ m^2 s^{-1} is the molecular diffusion coefficient of glycerol in water (D'Errico *et al.* 2004). We fixed $t_1 = 100$ s so that the amount of diffusion is the same for all the experiments and different $\bar{r}_0$ is obtained by varying Q_1 only. For example, $\bar{r}_0 = 15$, 18 and 20 mm were obtained by using $Q_1 = 3.3868$, 4.9121 and 6.086 µl s^{-1}, respectively.

As soon as the required dimensional radius $\bar{r}_0$ was reached, the flow rate was increased to Q^* and the less-viscous fluid was continuously injected at this flow up to a final time fixed for all the experiments. We repeated a series of experiments with $Q^* \in [0.05, 0.5]$ ml s^{-1}, $M \in [0, 2.053]$, and capture suppression of the fingering instability for different values of Q^* and M qualitatively similar to NLS. No instability was observed for many Q^* suggesting that there always exists a stable zone for each $\bar{r}_0$ as predicted by NLS for a range of Pe and shown in figure 5. The experimental images at various time for $\bar{r}_0 = 18$ mm and different M and Q^* are shown in figure 7. The effect of Pe or Q^* on the fingering dynamics is evident. For $Q^* = 0.1$ ml s^{-1}, the interface is slightly distorted near the final time, while $Q^* = 0.5$ ml s^{-1} shows VF instability. In addition, increasing M results in longer fingers and early onset as evident by comparing figures 7(*a*) and 7(*b*). The less-viscous fluid is dyed with Brilliant blue (BLENDS Ltd) food coloring dye to provide the visible contrast or optical observation to distinguish the two fluids. The amount of dye used is 0.01 g ml^{-1} in the solution and has a negligible effect on viscosity.

The controlling effect of the initial radius r_0 for $Q^* = 0.4$ ml s^{-1} and $M = 1.521$ is depicted in figure 8. We only show one quarter of the experimental images processed in MATLAB for better clarity. In addition, the validity of the control measure is justified on comparing with the experimental images for the point source ($r_0 = 0$) in figure 8(*a*). For visualisation purposes, we show the contours (plotted using the in-built command imcontour in MATLAB) of one quarter of the experimental images

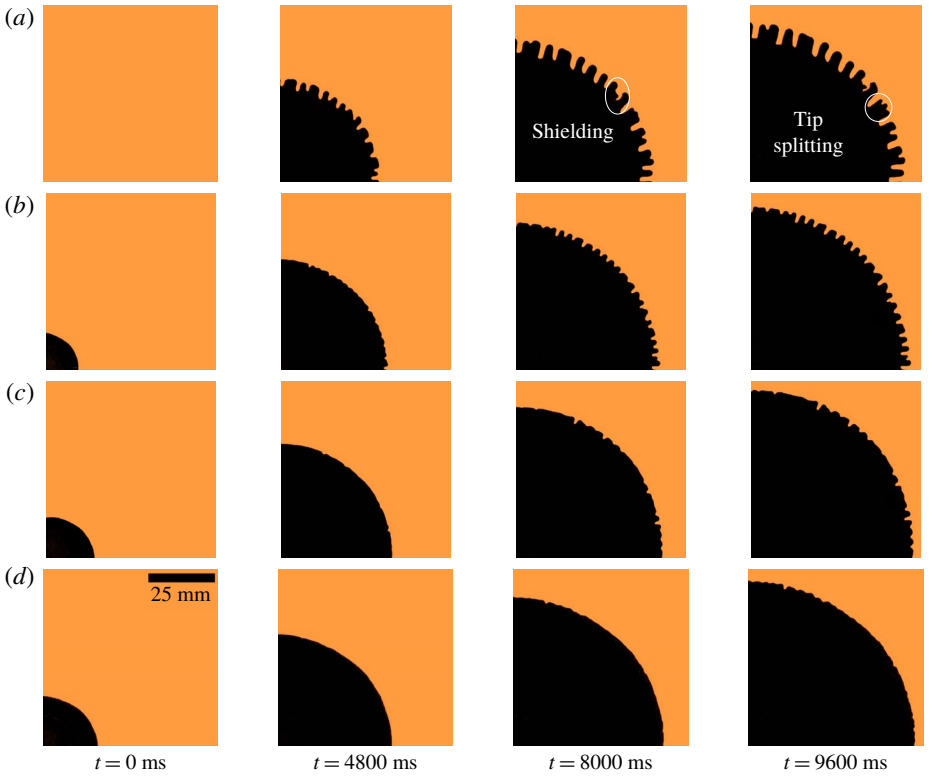

FIGURE 8. Experimental images at $t = 0$, 4800, 8000 and 9600 ms for $\bar{r}_0 =$ (*a*) 0 (point source), (*b*) 15, (*c*) 18 and (*d*) 20 mm. Tip splitting and shielding are observable for $\bar{r}_0 = 0$ and are significantly absent for $\bar{r}_0 \neq 0$. An abated instability with an increase in $\bar{r}_0$ is evident. A delay in instability is clearly visible on comparison of the snapshots for different $\bar{r}_0$. Here $Q^* = 0.4$ ml s^{-1} and $M = 1.521$.

in figure 9(*a*). A delayed onset and reduced fingering corresponding to $\bar{r}_0 = 20$ mm compared with $\bar{r}_0 = 15$ mm for $Q^* = 0.4$ ml s^{-1}, and $M = 1.521$ are evident. This supports the fact that the larger the $\bar{r}_0$, the weaker the advection and, hence, the initial competition between advection and diffusion determines the instability.

We use ImageJ (Schneider, Rasband & Eliceiri 2012) to quantify the experimental results. To avoid the noise induced by the presence of the injection pipes in the images, we utilise half of the experimental domain in our analysis. For the validity of the control measure, the experiments should capture the initial radial displacement in the form of a circular displacing front. Circularity is used as a measure of the extent up to which the displacement front is circular (Escala *et al.* 2019). We define the circularity as

$$C(t) = 2\pi A(t)/P^2(t), \tag{5.1}$$

where $A(t)$ and $P(t)$ correspond to the area and the perimeter of the region occupied by the less-viscous fluid, respectively, so that $C(t) = 1$ for a semi-circle. For $P(t)$, we consider only the length of the curved surface since the diameter does not contribute to $C(t)$. Subject to experimental errors, $C(t)$ close to 1 but constant over a range of time implies a circular displacing front. The maiden deviation of the circularity from the constant value indicates distortions at the front and it marks the triggering

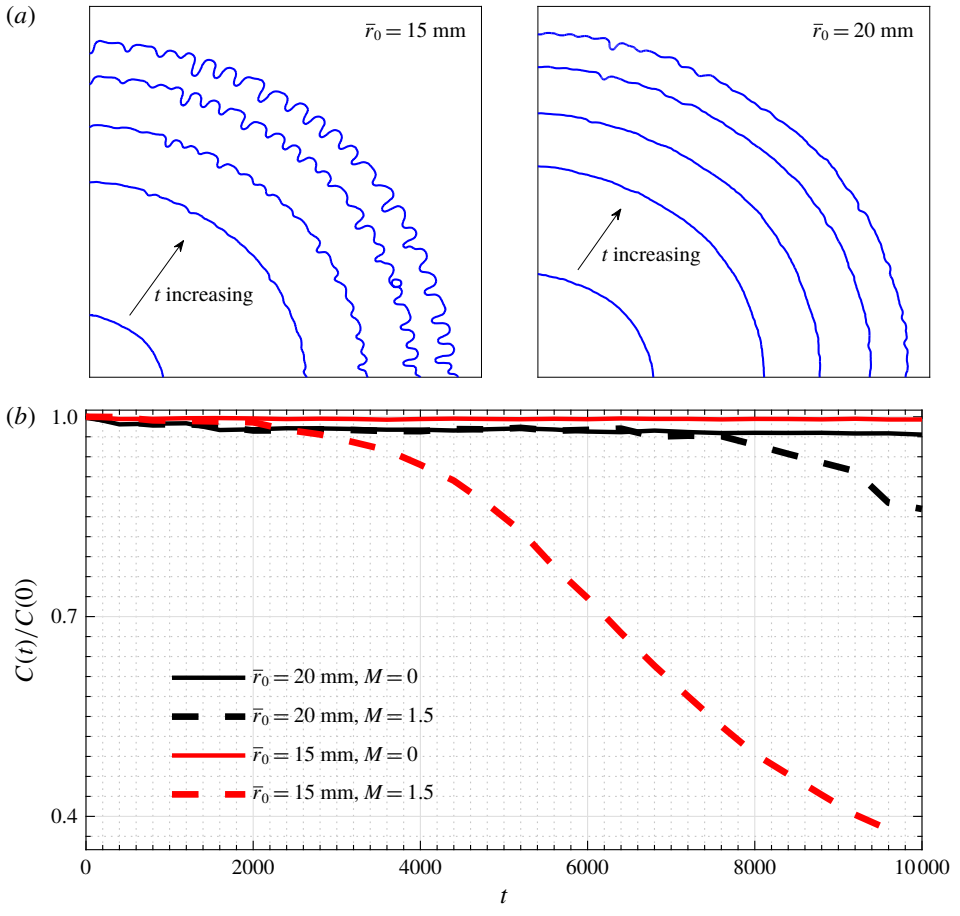

FIGURE 9. (*a*) Contours at $t = 0$, 4000, 6000, 8000 and 9600 ms of the experimental images (shown in figures 8*b* and 8*d* for $\bar{r}_0 = 15$ mm and $\bar{r}_0 = 20$ mm, respectively), showing the controlling effect of finiteness in terms of reduced and delayed instability. (*b*) Circularity as a function of time showing a delayed occurrence of distortions for larger $\bar{r}_0$.

of the instability. Here $M = 0$ works as the ideal radial source flow as no instability is observed as a result of equal viscosity of the two fluids. Hence, $C(t)$ for $M = 0$ is used as the reference constant value for each $\bar{r}_0$. We found that $C(t)$ for $M \neq 0$ deviates from the constant value after some initial time for each $\bar{r}_0$ and the time of deviation is larger for larger $\bar{r}_0$ (see figure 9*b* for $Q^* = 0.4$ ml s^{-1}). In other words, the instability is triggered later for a larger $\bar{r}_0$. This confirms the qualitative agreement of the experiments with LSA and NLS. The proposed control measure can be used to control VF in a wide variety of radial source flows with miscible fluids.

6. Discussion and conclusion

Depending upon the application, controlling fingering instabilities is of paramount importance, for instance, instability can increase mixing while it is detrimental to oil recovery or separation processes. VF in immiscible systems are controllable by modifying the geometry (Bongrand & Tsai 2018; Pihler-Puzović *et al.* 2018),

using time-dependent strategies (Dias *et al.* 2012; Zheng *et al.* 2015), which may be directly inapplicable in miscible VF (Huang & Chen 2015). In this article, we have investigated a stability mechanism in miscible VF by utilising the competition between the advective and diffusive forces.

Our theory takes care of the fact that the diffusive relaxation of the circular edge of the less-viscous inner fluid remains the same for all r_0 considered. This has been implemented by choosing the initial condition (2.4), which clearly indicates that there is no initial diffusive relaxation present in the model. The dominance of diffusion over weaker advection for larger r_0 is responsible for stability. On the other hand, in experiments, we inject the less-viscous fluid for 100 s at different flow rate Q_1 μl s^{-1} to achieve different $\bar{r}_0$. In this way, the diffusive relaxation of the edges of the circular region happens the same for all different initial conditions. This ensures that diffusion-dominating advection due to the weakening of the latter for larger $\bar{r}_0$ causes stability. To understand the stability by analyzing the competition between advection and diffusion, we have used energy amplification in LSA, interfacial length in NLSs and circularity in the experiments.

Using LSA and NLS, we have obtained a criterion to control radial miscible VF and have shown that the radius of the initial circular region containing the displacing fluid is a control parameter. No modification in the geometry or a continuous variation in the flow rate is required unlike in many other earlier studies of immiscible VF (Dias *et al.* 2012; Zheng *et al.* 2015). Our theoretical results have been compared with experiments that are in qualitative agreement with the numerical results.

Time-dependent strategies, such as changing the flow rate in a rectilinear configuration (Yuan *et al.* 2019) or varying the gap width of the Hele-Shaw cell in a radial configuration (Chen *et al.* 2010), have been attempted numerically in the context of miscible VF. Nevertheless, these studies lack sufficient evidence for the complete suppression of instability and have not validated experimentally. In contrast, we have successfully generated a stable radial experiment in accordance with our stability analysis and numerical simulations.

LSA predicts a delayed onset of instability with increasing r_0, whereas NLSs predict a critical log-mobility ratio M_c up to which there is no instability, dividing the M–Pe plane into stable and unstable zones for each r_0. The log-mobility ratio and Péclet number on the boundary of the stable and unstable zones scale as $M_c = 30(1 + 10r_0)Pe_c^{-0.55}$. The stable zone increases with increasing r_0. Taking $r_0 \to 0$ we approximate the critical Pe for a point source radial flow, which, for a mobility ratio of 3, is $\approx$65.8, that is of the same order as estimated from linear stability by Tan & Homsy (1987). For fixed values of Pe and M, it is concluded that a stable displacement for a given r_0 ensures a stable displacement for all larger r_0 despite a favourable viscosity gradient. On the other hand, an unstable displacement for a given r_0 indicates a stronger and early instability for all smaller r_0 keeping M and Pe fixed. This corresponds to weakening of advection with an increase in the distance from the source. Experiments performed demonstrate the validity and the applicability of the proposed control strategy.

In addition to helping to understand the intrinsic properties of fundamental hydrodynamic instabilities (Paterson 1981; Tan & Homsy 1987; Bischofberger *et al.* 2014) and pattern formation (Witten & Sander 1981; Li *et al.* 2009), our results suggest that the controllability of miscible VF in a radial configuration could be important in predicting the effectiveness of enhanced oil recovery by polymer flooding (Lake 1989) and in various other similar configurations.

Acknowledgements

M.M. acknowledges the financial support from SERB, Government of India through project grant no. MTR/2017/000283. S.P. acknowledges the support of the Swedish Research Council grant no. 638-2013-9243. C.-Y.C. is thankful to ROC (Taiwan) Ministry of Science and Technology, for financial support through grant no. MOST 107-2221-E-009-070-MY3. V.S. acknowledges NCTU Taiwan Elite Internship Program for the financial support to visit C.-Y.C.

Declaration of interests

The authors report no conflict of interest.

REFERENCES

AMOOIE, M. A., SOLTANIAN, M. R. & MOORTGAT, J. 2017 Hydrothermodynamic mixing of fluids across phases in porous media. *Geophys. Res. Lett.* **44** (8), 3624–3634.

BALL, T. V. & HUPPERT, H. E. 2019 Similarity solutions and viscous gravity current adjustment times. *J. Fluid Mech.* **874**, 285–298.

BHASKAR, K. R., GARIK, P., TURNER, B. S., BRADLEY, J. D., BANSIL, R., STANLEY, H. E. & LAMONT, J. T. 1992 Viscous fingering of HCl through gastric mucin. *Nature* **360**, 458–461.

BISCHOFBERGER, I., RAMACHANDRAN, R. & NAGEL, S. R. 2014 Fingering versus stability in the limit of zero interfacial tension. *Nat. Commun.* **5**, 5265.

BONGRAND, G. & TSAI, P. A. 2018 Manipulation of viscous fingering in a radially tapered cell geometry. *Phys. Rev.* E **97**, 061101(R).

CALLAN-JONES, A. C., JOANNY, J.-F. & PROST, J. 2008 Viscous-fingering-like instability of cell fragments. *Phys. Rev. Lett.* **100**, 258106.

CHEN, C.-Y., HUANG, C.-W., WANG, L.-C. & MIRANDA, J. A. 2010 Controlling radial fingering patterns in miscible confined flows. *Phys. Rev.* E **82**, 056308.

CHENG, N.-S. 2008 Formula for the viscosity of a glycerol–water mixture. *Ind. Engng Chem. Res.* **47** (9), 3285–3288.

CHUI, J. Y. Y., DE ANNA, P. & JUANES, R. 2015 Interface evolution during radial miscible viscous fingering. *Phys. Rev.* E **92**, 041003(R).

D'ERRICO, G., ORTONA, O., CAPUANO, F. & VITAGLIANO, V. 2004 Diffusion coefficients for the binary system glycerol + water at 25 °C. A velocity correlation study. *J. Chem. Engng Data* **49** (6), 1665–1670.

DIAS, E. O., ALVAREZ-LACALLE, E., CARVALHO, M. S. & MIRANDA, J. A. 2012 Minimization of viscous fluid fingering: a variational scheme for optimal flow rates. *Phys. Rev. Lett.* **109**, 144502.

ESCALA, D. M., DE WIT, A., CARBALLIDO-LANDEIRA, J. & MUÑUZURI, A. P. 2019 Viscous fingering induced by a pH-sensitive clock reaction. *Langmuir* **35** (11), 4182–4188.

GUIOCHON, G., FELINGER, A., SHIRAZI, D. G. & KATTI, A. M. 2008 *Fundamentals of Preparative and Nonlinear Chromatography*, 2nd edn. Academic Press Elsevier.

HOMSY, G. M. 1987 Viscous fingering in porous media. *Annu. Rev. Fluid Mech.* **19** (1), 271–311.

HOTA, T. K., PRAMANIK, S. & MISHRA, M. 2015*a* Nonmodal linear stability analysis of miscible viscous fingering in porous media. *Phys. Rev.* E **92**, 053007.

HOTA, T. K., PRAMANIK, S. & MISHRA, M. 2015*b* Onset of fingering instability in a finite slice of adsorbed solute. *Phys. Rev.* E **92**, 023013.

HUANG, Y.-S. & CHEN, C.-Y. 2015 A numerical study on radial Hele-Shaw flow: influence of fluid miscibility and injection scheme. *Comput. Mech.* **55** (2), 407–420.

JHA, B., CUETO-FELGUEROSO, L. & JUANES, R. 2011 Fluid mixing from viscous fingering. *Phys. Rev. Lett.* **106**, 194502.

LAKE, L. W. 1989 *Enhanced Oil Recovery*. Prentice-Hall.

LELE, S. K. 1992 Compact finite difference schemes with spectral-like resolution. *J. Comput. Phys.* **103** (1), 16–42.

LI, Q., CAI, W., LI, F.-C., LI, B. & CHEN, C.-Y. 2019 Miscible density-driven flows in heterogeneous porous media: influences of correlation length and distribution of permeability. *Phys. Rev. Fluids* **4**, 014502.

LI, S., LOWENGRUB, J. S., FONTANA, J. & PALFFY-MUHORAY, P. 2009 Control of viscous fingering patterns in a radial Hele-Shaw cell. *Phys. Rev. Lett.* **102**, 174501.

MATAR, O. K. & TROIAN, S. M. 1999 Spreading of a surfactant monolayer on a thin liquid film: onset and evolution of digitated structures. *Chaos* **9** (1), 141–153.

MISHRA, M., MARTIN, M. & DE WIT, A. 2008 Differences in miscible viscous fingering of finite width slices with positive or negative log-mobility ratio. *Phys. Rev.* E **78**, 066306.

MOORTGAT, J. 2016 Viscous and gravitational fingering in multiphase compositional and compressible flow. *Adv. Water Resour.* **89**, 53–66.

PATERSON, L. 1981 Radial fingering in a Hele-Shaw cell. *J. Fluid Mech.* **113**, 513–529.

PIHLER-PUZOVIĆ, D., PENG, G. G., LISTER, J. R., HEIL, M. & JUEL, A. 2018 Viscous fingering in a radial elastic-walled Hele-Shaw cell. *J. Fluid Mech.* **849**, 163–191.

PRAMANIK, S. & MISHRA, M. 2015 Effect of Péclet number on miscible rectilinear displacement in a Hele-Shaw cell. *Phys. Rev.* E **91**, 033006.

RIAZ, A., PANKIEWITZ, C. & MEIBURG, E. 2004 Linear stability of radial displacements in porous media: influence of velocity-induced dispersion and concentration-dependent diffusion. *Phys. Fluids* **16** (10), 3592–3598.

SCHNEIDER, C. A., RASBAND, W. S. & ELICEIRI, K. W. 2012 NIH Image to ImageJ: 25 years of image analysis. *Nat. Meth.* **9**, 671–675.

SHARMA, V., PRAMANIK, S., CHEN, C.-Y. & MISHRA, M. 2019 A numerical study on reaction-induced radial fingering instability. *J. Fluid Mech.* **862**, 624–638.

TAN, C. T. & HOMSY, G. M. 1987 Stability of miscible displacements in porous media: radial source flow. *Phys. Fluids* **30** (5), 1239–1245.

VIDEBÆK, T. E. & NAGEL, S. R. 2019 Diffusion-driven transition between two regimes of viscous fingering. *Phys. Rev. Fluids* **4**, 033902.

VOLK, A. & KÄHLER, C. J. 2018 Density model for aqueous glycerol solutions. *Exp. Fluids* **59** (5), 75.

WITTEN, JR., T. A, & SANDER, L. M. 1981 Diffusion-limited aggregation, a kinetic critical phenomenon. *Phys. Rev. Lett.* **47**, 1400–1403.

YUAN, Q., ZHOU, X., WANG, J., ZENG, F., KNORR, K. D. & IMRAN, M. 2019 Control of viscous fingering and mixing in miscible displacements with time-dependent rates. *AIChE J.* **65** (1), 360–371.

ZHENG, Z., KIM, H. & STONE, H. A. 2015 Controlling viscous fingering using time-dependent strategies. *Phys. Rev. Lett.* **115**, 174501.